Cancer Chemother Pharmacol (2009) 63:615–625
DOI 10.1007/s00280-008-0774-y

ORIGINAL ARTICLE

Efficacy, pharmacokinetics, tisssue distribution, and metabolism of the Myc–Max disruptor, 10058-F4 [Z,E]-5-[4-ethylbenzylidine]-2-thioxothiazolidin-4-one, in mice

Jianxia Guo · Robert A. Parise · Erin Joseph · Merrill J. Egorin · John S. Lazo · Edward V. Prochownik · Julie L. Eiseman

Received: 10 March 2008 / Accepted: 9 May 2008 / Published online: 29 May 2008

Abstract
Objectives c-Myc is commonly activated in many human tumors and is functionally important in cellular proliferation, differentiation, apoptosis and cell cycle progression. The activity of c-Myc requires noncovalent interaction with its client protein Max. In vitro studies indicate the thioxothiazolidinone, 10058-F4, inhibits c-Myc/Max dimerization. In this study, we report the efficacy, pharmacokinetics and metabolism of this novel protein–protein disruptor in mice.
Methods SCID mice bearing DU145 or PC-3 human prostate cancer xenografts were treated with either 20 or 30 mg/kg 10058-F4 on a qdx5 schedule for 2 weeks for efficacy studies. For pharmacokinetics and metabolism studies, mice bearing PC-3 or DU145 xenografts were treated with 20 mg/kg of 10058-F4 i.v. Plasma and tissues were collected 5–1440 min after dosing. The concentration of 10058-F4 in plasma and tissues was determined by HPLC, and metabolites were characterized by LC-MS/MS.
Results Following a single iv dose, peak plasma 10058-F4 concentrations of approximately 300 μM were seen at 5 min and declined to below the detection limit at 360 min. Plasma concentration versus time data were best approximated by a two-compartment, open, linear model. The highest tissue concentrations of 10058-F4 were found in fat, lung, liver, and kidney. Peak tumor concentrations of 10058-F4 were at least tenfold lower than peak plasma concentrations. Eight metabolites of 10058-F4 were identified in plasma, liver, and kidney. The terminal half-life of 10058-F4 was approximately 1 h, and the volume of distribution was >200 ml/kg. No significant inhibition of tumor growth was seen after i.v. treatment of mice with either 20 or 30 mg/kg 10058-F4.
Conclusion The lack of significant antitumor activity of 10058-F4 in tumor-bearing mice may have resulted from its rapid metabolism and low concentration in tumors.

Keywords c-Myc · Cancer · c-Myc/Max inhibitor · Protein–protein disruptor · Thioxothiazolidinone

J. Guo · R. A. Parise · E. Joseph · M. J. Egorin · J. L. Eiseman (✉)
Hillman Cancer Center,
The University of Pittsburgh Cancer Institute,
Room G27b. 5117 Centre Ave., Pittsburgh, PA 15213, USA
e-mail: eisemanj@msx.upmc.edu; eisemanj@upmc.edu

J. S. Lazo
Department of Pharmacology,
The University of Pittsburgh Cancer Institute,
Room G27b. 5117 Centre Ave., Pittsburgh, PA 15213, USA

E. V. Prochownik
Section of Hematology/Oncology,
Children's Hospital, Pittsburgh, PA, USA

Introduction

The c-Myc protein is a transcription factor, which is encoded by the c-Myc gene on human chromosome 8q24, plays important roles in cell proliferation, growth, cell cycle progression, genomic stability, differentiation, and apoptosis [1]. c-Myc/Max protein complexes bind to DNA to activate transcription and induce cell transformation.

Abnormalities of c-Myc oncoprotein expression are observed with high frequency in lymphoid malignancies, especially Burkitt's lymphoma and leukemia, and in breast, colon, and prostate cancers [2–12]. c-Myc is amplified in approximately 40% of prostate cancers, and this amplification is associated with progression [9, 10]. In androgen-independent prostate cancer, c-Myc is deregulated in approximately 70% of evaluated cases, and c-Myc amplification is observed after androgen ablation therapy [13].

Androgen-independent prostate cancers do not respond to androgen ablation therapies and are poorly responsive to standard chemotherapies. There is a need to develop novel therapeutic strategies for their treatment. Because the c-Myc oncoprotein is overexpressed in prostate cancer, c-Myc is an attractive target for novel anti-tumor therapies. Several groups have used oligonucleotides to interfere with c-Myc gene expression [14], and antisense oligonucleotides to inhibit its translation in experimental models [12]. However, translating these approaches into practical clinical therapies has not yet been successful. Small molecule disruptors of the c-Myc/Max heterodimer complex have previously been identified in vitro and represent attractive alternatives to nucleic acid-based methods [1, 15].

The thioxothiazolidinone, 10058-F4, is among the first compounds found to disrupt the association between c-Myc and Max [1]. Gomez-Curet et al. reported that 10058-F4 not only blocked c-Myc function through the mechanism of c-Myc/Max heterodimer dissociation, but also decreased c-Myc mRNA levels in lymphoma cells [7]. Huang et al. [8] showed that 10058-F4 arrested AML cells at the G0/G1 interface, downregulated c-Myc expression, and upregulated the CDK inhibitors, p21 and p27. In addition, 10058-F4 induced apoptosis through activation of a mitochondrial pathway, as shown by downregulation of Bcl-2, upregulation of Bax, release of cytoplasmic cytochrome C, and cleavage of caspase 3, 7, and 9. 10058-F4 also induced myeloid differentiation, possibly through activation of multiple transcription factors. Similarly, 10058-F4 induced apoptosis and differentiation was also observed in primary AML cell cultures. Lin et al. [9] demonstrated that 10058-F4 arrested hepatocellular carcinoma cells at G0/G1 phase of the cycle and significantly decreased alpha-fetoprotein levels, an indicator of differentiation. Most recently, Sampson et al. [9] demonstrated that, in addition to promoting c-Myc/Max dissociation, 10058-F4 also inhibited c-Myc protein expression. Together these effects resulted in the down-regulation of c-Myc target gene expression in Namalwa Burkitt lymphoma cells. Because of these interesting in vitro results, we investigated the preclinical pharmacology of 10058-F4 in SCID mice bearing androgen-independent, human prostate cancer xenografts.

Materials and methods

Reagents

Acetonitrile (HPLC-grade) and water (HPLC-grade) were purchased from Fisher Scientific (Fairlawn, NJ, USA). Nitrogen gas and liquid nitrogen were purchased from Valley National Gases Inc. (Pittsburgh, PA, USA). Ammonium acetate and Cremophor EL were purchased from Sigma–Aldrich (St Louis, MO, USA). 10058-F4 ([Z, E]-5-[4-ethylbenzylidine]-2-thioxothiazolidin-4-one, 5404711) was obtained from Chembridge Corporation (San Diego, CA, USA). Fenretinide (4-HPR) was obtained from CTEP, NCI (Rockville, MD, USA). Dextrose (5%) for injection, saline (0.154 M NaCl) and sterile water were purchased from Baxter Healthcare Corporation (Deerfield, IL, USA). Ethanol (200 Proof) was purchased from Pharmaco Products (Brookfield, CT, USA). Docetaxel (Taxotere® Sanofi Aventis, injection concentrate) was purchased from the University of Pittsburgh Cancer Institute Pharmacy. Nitrogen gas for the mass spectrometer was generated with a 75-880 generation system (Parker Balston, Columbus, OH, USA).

Dosing solutions

Dosing solutions were prepared by dissolving 10058-F4 in cremophor EL:ethanol:saline (1:1:8 v/v/v) at a final concentration of 2 or 3 mg/ml. Docetaxel was diluted to 1 mg/ml with saline.

Mice

Specific-pathogen-free, female SCID mice (5–6 weeks of age) were obtained from the Animal Program administered by the Biological Testing Branch of the National Cancer Institute (Frederick, MD, USA). Mice were allowed to acclimate to the University of Pittsburgh Animal Facility for at least 1 week before studies were initiated. To minimize exogenous infection, mice were maintained in microisolator cages and handled in accordance with the Guide for the Care and Use of Laboratory Animals (National Research Council, 1996). Ventilation and airflow in the animal facility were set to 12 changes/h. Room temperature was regulated at 72 ± 2°F, and the rooms were kept on automatic 12-h light/dark cycles. The mice received Prolab ISOPRO RMH 3000, Irradiated Lab Diet (PMI Nutrition International, Brentwood, MO, USA) and water ad libitium except on the evening prior to dosing for the pharmacokinetic studies, when all food and water was removed and withheld until 4 h after dosing. Sentinel animals (CD-1 mice in cages with bedding 20% of which was bedding removed from the study animal cages at cage change) were maintained in the room housing the study animals and assayed at monthly intervals for specific murine pathogens by murine antibody profile testing (Charles River, Boston, MA, USA). Sentinel animals remained free of specific pathogens throughout the study period, implying that the study animals were free of specific pathogens.

Tumor cell lines

DU145 and PC-3 human androgen-independent prostate cancer cells were obtained from ATCC (Manassas, VA,

USA) and expanded in RPMI 1640 medium (Gibco®, Invitrogen, Carlsbad, CA, USA), containing 10% heat-inactivated fetal bovine serum (Biofluids™, Biosource, Rockville, MD, USA) and 10 μg/ml gentamycin (Gibco®, Invitrogen, Carlsbad, CA, USA) in an incubator with 95% air, 5% CO_2, 95% humidity at 37°C.

MTT assay

PC-3 cells (2×10^4 cells in logarithmic growth) were plated into 96-well culture plates and allowed to adhere to the plates for 24 h prior to the addition of 10058-F4 in medium containing 1% ethanol such that the final concentrations in the wells were 0.1–100 μM in medium containing 0.3% ethanol. After 72 h, 50 μl of 1 mg/ml MTT was added to each well. The cells were washed with medium and phosphate buffered saline, and 150 μl of DMSO was added to each well, followed by shaking for 5 min. The absorbance at 570 nm was read on DYNEX MRX Revelation microplate reader (Dynex, Vienna, VA, USA). Results were compared to wells containing cells treated with vehicle alone and were expressed as % inhibition. The IC_{50} was calculated using the Hill equation, the program ADAPT II [16], and data from three separate experiments.

Tumor implantation

PC-3 or DU145 cells (5×10^6 cells in logarithmic growth) were injected subcutaneously into the right flank of passage SCID mice before implantation into study animals. When the tumors reached approximately 500 mm^3, passage mice were euthanized with CO_2, and the tumors harvested aseptically. The harvested tumors were cut into approximately 25-mm^3 fragments and implanted subcutaneously on the right flanks of study mice. When the tumors in the study mice were approximately 300 mm^3, the animals were stratified into treatment groups of 5 animals each for the study in mice bearing PC-3 xenografts and 8 mice per treatment group in the study in mice bearing DU145 xenografts, such that at the start of each study there were no differences in mean body weights or tumor volumes between the various treatment groups.

Efficacy studies

C B-17 SCID mice bearing PC-3 human prostate tumor xenografts were stratified into the following groups: Control, vehicle control, positive control (docetaxel, 10 mg/kg), and 10058-F4 treatment (20 or 30 mg/kg/dose). Previous studies by us indicated that 30 mg/kg was the maximally tolerated dose of 10058-F4 on this schedule (data not shown). Mice were treated i.v. daily for 5 days for 2 weeks, and body weights and tumor volumes were recorded twice weekly. In the second study, C B-17 SCID mice bearing DU145 human androgen-independent prostate cancer xenografts were stratified to similar treatment groups. Docetaxel served as the positive control for both efficacy studies and was administered i.v. every 7 days for two doses of 10 mg/kg. Tumors were measured with calipers, and tumor volumes were calculated using the formula: $TV = L \times W^2/2$ where L is the largest diameter of the tumor and W is the smallest diameter perpendicular to L. Mice were followed for at least 1 week following the completion of the dosing so that tumor regrowth could be monitored.

Pharmacokinetic studies

C B-17 SCID mice bearing PC-3 or DU145 xenografts (3 per time point) were fasted overnight and treated with 10058-F4 at a dose of 20 mg/kg i.v. Mice were euthanized at the following times after dosing: 5, 10, 15, 30, 45, 60, 120, 240, 360, 420 and 1,440 min after 10058-F4 or 5 min after vehicle administration. Control mice and 10058-F4-treated mice bearing DU145 xenografts in the 1,440 min time point group were housed in metabolism cages, and separate urine and feces collections were obtained at 0–7 and 7–24 h. Mice were euthanized by CO_2 inhalation, and blood was collected by cardiac puncture using heparinized syringes and needles. The following tissues were collected, weighed and snap frozen in liquid nitrogen:liver, kidney, lung, spleen, heart, brain, skeletal muscle, and fat from mice bearing DU 145 xenografts, while only liver, kidney, lung, and tumor were collected from mice bearing PC-3 xenografts. Blood was centrifuged at $12{,}000 \times g$ for 4 min to obtain plasma and red blood cells. All samples, including excreta, were stored at −70°C until analysis.

Plasma, urine, and tissue sample preparation

Plasma and urine samples were extracted directly. Tissue samples were homogenized in five volumes of phosphate-buffered saline (pH 7.4). To a 200 μl sample of plasma, urine, red blood cells, or tissue homogenate, 5 μl of 10 μg/ml 4-HPR was added as an internal standard. Proteins were precipitated with 1 ml acetonitrile followed by mixing for 15 s on a Vortex Genie 2 (model G560, Scientific Industries, Bohemia, NY, USA) set at 4. Samples were subsequently centrifuged at $13{,}000 \times g$ for 10 min, and the supernatants were transferred to 12 × 75 mm glass tubes and evaporated to dryness under a stream of nitrogen. Each dried residue was resuspended in 300 μl of 10% acetonitrile, and 100 μl of each resuspended sample was injected onto the HPLC.

HPLC analysis

HPLC was performed on a Waters 2695 separation system (Waters Corp., Milford, MA, USA) fitted with a 4.6 × 100 mm, 5 μm Luna C18 (2) column (Phenomenex,

Torrance, CA, USA) and Brownlee C18 guard column (PerkinElmer, Shelton, CT, USA) that were perfused with a gradient mobile phase that consisted of a linear gradient from acetonitrile:10 mM ammonium acetate (10:90, v/v) to 100% acetonitrile over 15 min followed by a 5-min isocratic period. The mobile phase was pumped at flow rate of 1 ml/min. Column eluate absorbance at 382 nm was monitored with a Waters 2487 Dual absorbance detector. Under these conditions, the retention times of 10058-F4 and the internal standard were approximately 11.3 and 16.8 min, respectively. Standard curves of 10058-F4 at concentrations of 0.03–10 μg/ml in plasma, or control tissue homogenates were prepared in triplicate. The 10058-F4-to-internal standard ratio was calculated for each standard by dividing the area of each analyte peak by the area of the respective internal standard peak for that sample. Standard curves of 10058-F4 were constructed by plotting the 10058-F4-to-internal standard ratio versus the known concentration of 10058-F4 in each sample. Standard curves were fitted by linear regression followed by back calculation of concentrations. Concentrations in unknown samples were calculated by comparison with the appropriate standard curve of area ratios of 10058-F4 to internal standard. The lower limit of quantification of 10058-F4 was 0.01 μg/ml. Coefficients of variation in plasma at a low mid-range concentration (0.1 μg/ml) and high mid-range concentration (3 μg/ml) was 2.56 and 4.11%, respectively. Recoveries of 10058-F4 from plasma containing 3 and 30 μg/ml were 82.68 ± 1.09 and 93.38 ± 0.79%, respectively.

Pharmacokinetic analysis

The plasma concentration versus time data of 10058-F4 were analyzed using the program ADAPT II [16] with maximum likelihood estimation. Compartmental models were fit to the data from i.v. pharmacokinetic studies, and model discrimination was based on Akaike's Information Criterion [17]. Parameter values for the volume of the central compartment (V_c), the elimination rate constant k_e and transfer constants, such as k_{pc} and k_{cp}, were estimated. The areas under the concentration (AUC) versus time curves for plasma and tissues were estimated by noncompartmental analysis using the program LAGRAN and the Lagrange function [18].

Metabolite analysis by LC-MS/MS

Mice were euthanized by CO_2 inhalation 30 min after treatment with 20 mg/kg of 10058-F4 i.v. Plasma, liver and kidneys were collected and processed as described for pharmacokinetic studies and then analyzed by LC-MS/MS as described below.

LC-MS/MS

The HPLC system consisted of an Agilent (Palo Alto, CA, USA) 1100 autosampler and binary pump, a Phenomenex (Torrance, CA, USA) Luna C18 (2) (5 μm, 2 × 150 mm) column kept at ambient temperature, and a gradient mobile phase. The gradient mobile phase consisted of solvent A: 0.1% (v/v) formic acid in acetonitrile, and B: 0.1% (v/v) formic acid in water. The initial mobile phase of 10% solvent A and 90% solvent B was increased linearly for 30 min to 100% A, at a flow rate of 0.2 ml/min. These conditions were maintained for 5 min. The gradient was returned to initial conditions at 36 min. The run time was 45 min. Mass spectrometry was performed with a Micromass (Milford, MA, USA) Quattromicro triple-stage, bench-top mass spectrometer operated in single quadrupole mode. The mass spectrometer was operated using both electrospray positive and negative ionization with the following conditions: capillary voltage of 3.0 kV, cone voltage of 20 V, source temperature of 120°C, desolvation temperature of 450°C, and cone and desolvation gas flow of 110 and 550 L/h, respectively. The eluate was monitored from 200 to 600 *m/z*. The data was collected by Masslynx version 4.0 (Micromass, Milford, MA, USA).

Pharmacodynamic study

c-Myc and Max expression in DU145 or PC-3 tumor samples were examined by western blot. Mice bearing either DU145 or PC-3 xenografts were treated with 20 mg/kg 10058-F4 i.v. and tumor samples were collected at 2, 4, 6, or 24 h after i.v. dosing. Protein extracts were prepared by homogenizing thawed tissues in ten volumes of lysis buffer [50 mM Tris–HCl (pH 7.9), 2 mM EDTA, 100 mM NaCl, 1% NP-40, 10 mM NaF, 10 mM sodium vanadate] containing freshly prepared protein inhibitors [1 μg/ml pepstatin, 10 μg/ml aprotin, 5 μg/ml leupeptin, 5 mM PMSF, 0.1 μM microcystin and 5 mM Na pyrophosphate (BD Biosciences Pharmingen, San Diego, CA, USA)] using an Omni Tissuemizer (Omni International, Westbury, CT, USA). Each tissue lysate was centrifuged at 12,000×*g* for 10 min. The resulting supernatants were collected and protein concentration was measured with the Bio-Rad protein assay system (Bio-Rad, Hercules, CA, USA). Concentrations of bovine albumin between 0.05 and 0.5 mg/ml were used to obtain a calibration curve. Equal amounts of protein (40 μg) were denatured in Laemmli sample buffer containing 0.4 M Tris–HCl (pH 6.8), 8% SDS, 39% glycerol, 0.04% bromophenyl blue and 0.4 M dithiotreitol (Bio-Rad) and loaded on 4–15% gradient gels (Bio-Rad). The separated proteins were transferred onto PVDF membranes and blotted with 5% non-fat milk in Tris–Buffered Saline for 1 h. The membranes were then incubated with antibodies against c-Myc

(9E10) or Max (C-124) (Santa Cruz Biotechnology, Inc. Santa Cruz, CA, USA) overnight at 4°C. Glyceraldahyde-3-phosphate dehydrogenase (GAPDH) (MAB374, Chemicon International, Temecula, CA, USA) expression was used as a loading control. The immunoreactive signals were detected by ELC detection reagents (PerkinElmer Life Sciences, Boston, MA, USA) following the manufacturer's instructions. The densities of the signal were quantified by densitometry with UN-SCAN-IT (Silk Scientific, Orem, UT, USA).

Statistics

The mean data were analyzed using ANOVA with pairwise comparisons made using Dunnett's test. Nonparametric analysis of median data was performed using Kruskall–Wallace and pairwise comparisons were conducted with the Mann–Whitney test. Significance was set at $P \leq 0.05$. The statistical package used was Minitab (State College, PA, USA).

Results

In vitro cytotoxicity

The IC_{50} values of 10058-F4 against cultured PC-3 and DU145 cells determined at 72 h after a single addition of the drug were estimated using the Hill equation to be 113 ± 30 and 88 ± 20 μM, respectively.

Efficacy

Treatment of SCID mice bearing DU145 or PC-3 xenografts with either the maximally tolerated dose of 30 or 20 mg/kg 10058-F4 on a qdx5 schedule for 2 weeks did not inhibit tumor growth significantly (Fig. 1). The maximum mean %TC values (% treated tumor/control tumor volume) on day 18 for the mice bearing PC-3 xenografts treated with 20 or 30 mg/kg 10058-F4 were 72.3 and 72.9%, respectively. In contrast, intravenous treatment with 10 mg/kg docetaxel on a q7dx2 schedule resulted in significant tumor growth inhibition and a maximum mean %T/C of 20.2% on day 18. Similar lack of response to treatment with 10058-F4 was observed in mice bearing DU145 xenografts. The mean maximum %T/C following treatment with 30 mg/kg 10058-F4 was only 85% when compared to the vehicle-treated mice and only 67% when compared with the untreated control mice. In contrast, docetaxel treatment of mice bearing DU145 xenografts resulted in tumor regression and a %T/C of 2%. Although mice bearing PC-3 androgen-independent xenografts lost up to 18% body weight during the course of the study, this weight loss was consistent across all groups and appeared to be related to the tumor xenograft. No significant decreases in body weight were observed in the mice bearing DU145 xenografts during the course of treatment.

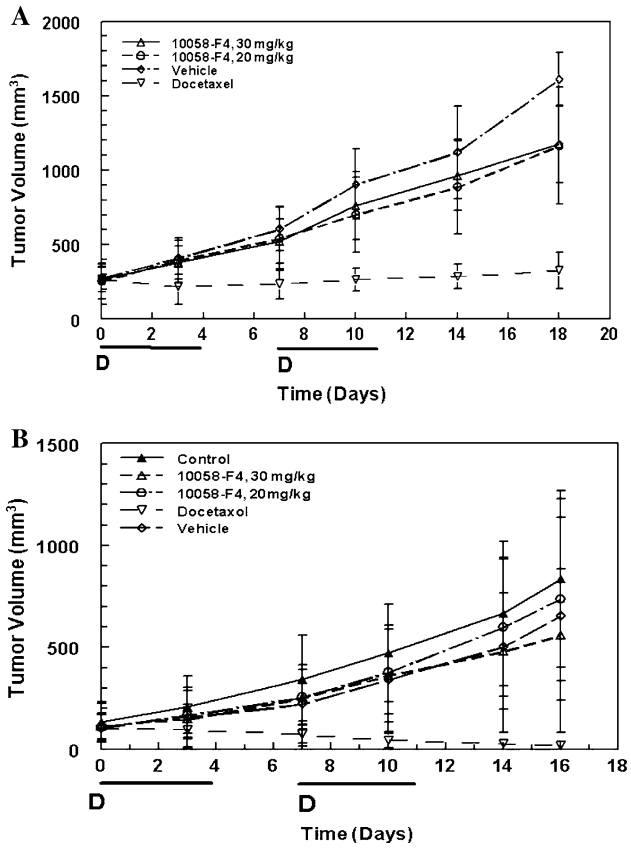

Fig. 1 Antitumor activity of 10058-F4 in mice bearing human PC-3 (**a**) or DU145 (**b**) tumor xenografts. Results are the mean ± SD tumor volumes of 5 animals or 8 animals for PC-3 and DU145, respectively. The days of treatment with 10058-F4 are indicated by the *bold line*. Days of docetaxel treatment are indicated by the symbol, *D*

Plasma pharmacokinetics of 10058-F4

The 10058-F4 plasma concentrations versus time data are presented in Fig. 2. Peak plasma concentrations of 10058-F4 occurred at 5 min in mice bearing DU145 xenografts or PC-3 xenografts and were 368.5 and 272.7 μM, respectively. Plasma concentrations of 10058-F4 decreased rapidly and were undetectable beyond 360 min after 10058-F4 administration. A two-compartment model best fit the plasma 10058-F4 concentrations versus time data, and the pharmacokinetic parameters associated with that model are presented in Table 1. The terminal half-life of 10058-F4 was approximately 1 h, and the volume of distribution was small, approximately 200 ml/kg. Clearance was rapid, >600 ml/h/kg.

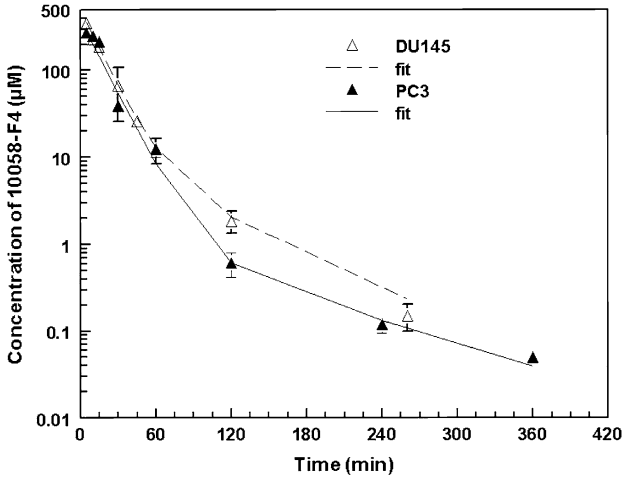

Fig. 2 Plasma Concentrations of 10058-F4 versus time in C B-17 SCID mice bearing PC-3 or DU145 xenografts treated i.v. with 20 mg/kg 10058-F4. *Symbols* are the mean ± standard deviation. The lines are the predicted fits obtained using the two compartment, open, linear model

Table 1 Pharmacokinetics parameters resulting from fitting of a two-compartment, open, linear model to plasma 10058-F4 concentration-versus-time data

Parameters	Mice bearing DU145 tumor (Mean ± SD)	Mice bearing PC-3 tumor (Mean ± SD)
Ke (h^{-1})	3.817 ± 0.229	3.825 ± 0.185
Kcp (h^{-1})	0.2459 ± 0.066	0.06958 ± 0.0145
Kpc (h^{-1})	1.044 ± 0.157	0.6191 ± 0.095
CLt (ml/h kg^{-1})	610.6 ± 39.89	808.0 ± 42.347
Vc (ml/kg)	160.0 ± 17.54	211.3 ± 18.079
α (h^{-1})	4.146 ± 0.292	3.907 ± 0.197
β (h^{-1})	0.9617 ± 0.123	0.6060 ± 0.091
t1/2-α (h)	0.1672 ± 0.012	0.1774 ± 0.089
t1/2-*β* (h)	0.7208 ± 0.096	1.144 ± 0.122

Vc volume of the central compartment, *Ke* elimination constant, *Kcp* transfer constant from the central to the peripheral compartment, *Kpc* from the peripheral compartment to the central compartment, *t1/2* terminal half-life, *CLt* total body clearance; α and *β* are the macroscopic rate constants for distribution and elimination, respectively

Urinary excretion of 10058-F4

Less than 0.1% of the dose of 10058-F4 was detected as unchanged 10058-F4 in the urine of mice bearing DU145 tumors. Only 0.02% was excreted during the first 7 h after administration, and 0.04% of the administered dose was accounted for in the 7–24 h urine samples.

Tissue concentrations of 10058-F4 following i.v. administration

After i.v. bolus delivery to mice, 10058-F4 distributed rapidly to all tissues (Tables 2, 3). Peak concentrations of

Table 2 Concentrations of 10058-F4 and AUC in plasma and tissues after administration of 20 mg/kg 10058-F4 i.v. to C B-17 SCID female mice bearing DU145 tumors

Time (Min)	Plasma (nmol/ml)	Tumor (nmol/g)	Liver (nmol/g)	Kidney (nmol/g)	Lung (nmol/g)	Spleen (nmol/g)	Heart (nmol/g)	Brain (nmol/g)	Skeletal Muscles (nmol/g)	RBC (nmol/ml)	Fat (nmol/g)
5	351.71 ± 49.53	10.09 ± 4.41	84.77 ± 16.51	56.48 ± 11.16	111.26 ± 6.44	45.32 ± 9.44	18.69 ± 9.73	17.70 ± 3.24	33.92 ± 7.99	46.14 ± 17.03	94.74 ± 18.73
10	228.12 ± 15.00	9.79 ± 4.91	45.79 ± 4.86	38.83 ± 1.17	72.28 ± 26.98	20.89 ± 14.78	11.94 ± 5.91	45.27 ± 4.44	22.36 ± 3.95	30.77 ± 9.97	51.56 ± 10.34
15	185.08 ± 25.57	14.44 ± 7.03	29.48 ± 10.21	21.02 ± 2.81	39.52 ± 5.12	22.00 ± 3.29	5.80 ± 2.49	4.77 ± 1.50	16.76 ± 2.89	15.06 ± 5.42	183.20 ± 10.31
30	66.90 ± 40.93	5.13 ± 1.99	6.63 ± 2.75	7.07 ± 1.52	22.58 ± 6.33	5.46 ± 2.99	2.70 ± 0.51	0.74 ± 0.27	6.97 ± 2.23	4.37 ± 0.69	46.38 ± 8.99
60	25.98 ± 4.21	5.05 ± 1.71	4.96 ± 1.58	3.48 ± 0.89	10.38 ± 7.04	1.32 ± 0.98	0.67 ± 0.18	0.08 ± 0.02	3.01 ± 0.13	3.06 ± 0.25	12.98 ± 4.40
120	12.32 ± 3.97	3.61 ± 0.76	ND	2.32 ± 0.68	3.08 ± 1.11	0.36 ± 0.15	0.20 ± 0.06	ND	1.60 ± 0.31	1.21 ± 0.28	7.23 ± 0.03
260	1.85 ± 0.51	1.50 ± 0.13	ND	ND	0.67 ± 0.12	ND	0.11 ± 0.05	ND	ND	0.12 ± 0.02	1.10 ± 0.02
360	0.15 ± 0.05	1.48	ND	ND	ND	ND	ND	ND	ND	ND	ND
AUC (nmol h/ml) or (nmol h/g)	133.40	25.02	19.38	19.33	37.83	11.52	4.73	3.60	13.32	13.28	80.05

Table 3 Concentrations of 10058-F4 and AUC in plasma and tissues after administration of 20 mg/kg 10058-F4 i.v. to C B-17 SCID female mice bearing PC-3 tumors

Time (Min)	Plasma (nmol/ml)	Tumor (nmol/g)	Liver (nmol/g)	Kidney (nmol/g)	Lung (nmol/g)	RBC (nmol/ml)
5	272.72 ± 27.84	7.98 ± 0.37	43.88 ± 7.50	59.55 ± 24.68	93.72 ± 2.61	41.29 ± 15.00
10	246.47 ± 27.54	7.13 ± 1.43	23.25 ± 0.49	28.84 ± 2.77	84.58 ± 19.08	27.84 ± 0.79
15	213.15 ± 13.99	7.51 ± 0.67	17.29 ± 0.81	25.51 ± 2.36	60.21 ± 4.29	14.15 ± 3.38
30	38.77 ± 1.69	3.96 ± 0.28	8.83 ± 0.35	5.82 ± 1.05	14.57 ± 0.19	8.24 ± 1.00
60	12.59 ± 2.63	2.91 ± 0.44	1.74 ± 0.04	2.09 ± 0.24	4.11 ± 0.13	3.06 ± 0.32
120	0.61 ± 0.19	1.48 ± 0.14	ND	ND	0.60 ± 0.01	0.16
240	0.12 ± 0.02	0.17 ± 0.03	ND	ND	ND	ND
360	0.05 ± 0.004	0.09 ± 0.01	ND	ND	ND	ND
AUC (nmol h/ml) or (nmol h/g)	88.81	8.33	12.55	13.87	29.17	12.60

10058-F4 in liver, kidney, lung, spleen, heart and skeletal muscle occurred at 5 min after administration, which was the earliest time point sampled. In mice bearing DU145 tumors, peak concentration of 10058-F4 in fat and brain occurred slightly later, at 15 and 10 min, respectively. The peak concentration of 10058-F4 in tumors was much lower than in other tissues. Concentrations in both DU145 and PC-3 xenografts were relatively constant between 5 and 15 min, and then decreased, so that they were not detectable at times beyond 6 h after i.v. drug delivery. The peak concentration in either tumor was only about 5% of the peak plasma concentration. The AUC's for the tissues, including tumor, were lower than the AUC for plasma (Tables 2, 3). In each case, <20% of the area was extrapolated beyond the last data point.

Pharmacodynamics

Expression of c-Myc and Max in tumor samples was analyzed by western blot at 2, 4, 24 h after administration of 10058-F4 at 20 mg/kg. In contrast to what might be predicted from cell culture results [8, 9], there were no significant changes in the concentrations of either c-Myc or Max compared to untreated control tumors (data not shown).

Metabolite analysis

After an i.v. dose of 20 mg/kg, additional, earlier-eluting peaks were observed in the plasma of mice treated with 10058-F4 (Fig. 3c) when compared with control plasma (Fig. 3 a) or control plasma to which10058-F4 and internal standard had been added (Fig. 3b). A small peak with a retention time of 12.2 min was present in the samples containing 10058-F4. This peak represented <5% of the area of 10058-F4 and appeared to be a contaminant in 10058-F4. This peak was present when 10058-F4 was added directly to mobile phase or to control plasma (Fig. 3b), and this peak was also present in the plasma of a mouse treated with 10058-F4 and euthanized 30 min after treatment.

The metabolites of 10058-F4 were further characterized using LC-MS/MS. Plasma and liver from a mouse killed 30 min after administration of 20 mg/kg 10058-F4 were extracted and analyzed by LC/MS-MS. Spectral comparisons were made with 10058-F4. While 3 additional compounds were detected in the HPLC chromatogram of the plasma obtained 30 min after iv administration of 20 mg/kg 10058-F4 (Fig. 3c), at least 8 potential metabolite peaks were detected using LC/MS-MS and their chromatograms are shown in Fig. 4b–i. As observed in Fig. 4a, 10058-F4 had a retention time of 27 min, while the contaminant had a retention time of 26 min. Although the contaminant had also had a mass to charge ratio of 248 and appeared to ionize better than 10058-F4, this contaminant also displayed a major mass to charge ratio of 540. None of the proposed metabolites were detected in the chromatograms from either control plasma or control liver.

As observed in Fig. 4b–i, the 8 additional compounds detected in plasma or liver of the 10058-F4 treated mouse had *m/z* ratios of 232 (plasma only), 248, 250, 264, 266, 280 (liver only), 282, and 298 using negative ionization. All potential metabolites were more polar than 10058-F4 and the proposed structures, displayed in Fig. 5, are consistent with metabolism by hydroxylation of either the aromatic ring or ethyl side chain, oxidative desulfuration and hydrolytic thioxothiazolidinone ring opening. Based on the chromatogram, the metabolite with a *m/z* ratio of 266, consistent with ring opening, appeared to be the most prevalent. There are three potential structures proposed for the metabolite having a *m/z* ratio of 264, however, in the chromatogram there appear to be only two major peaks.

Discussion

c-Myc plays an important role in the growth of cancer cells through its activation of numerous downstream pathways. Novel ways to inhibit c-Myc have been investigated and

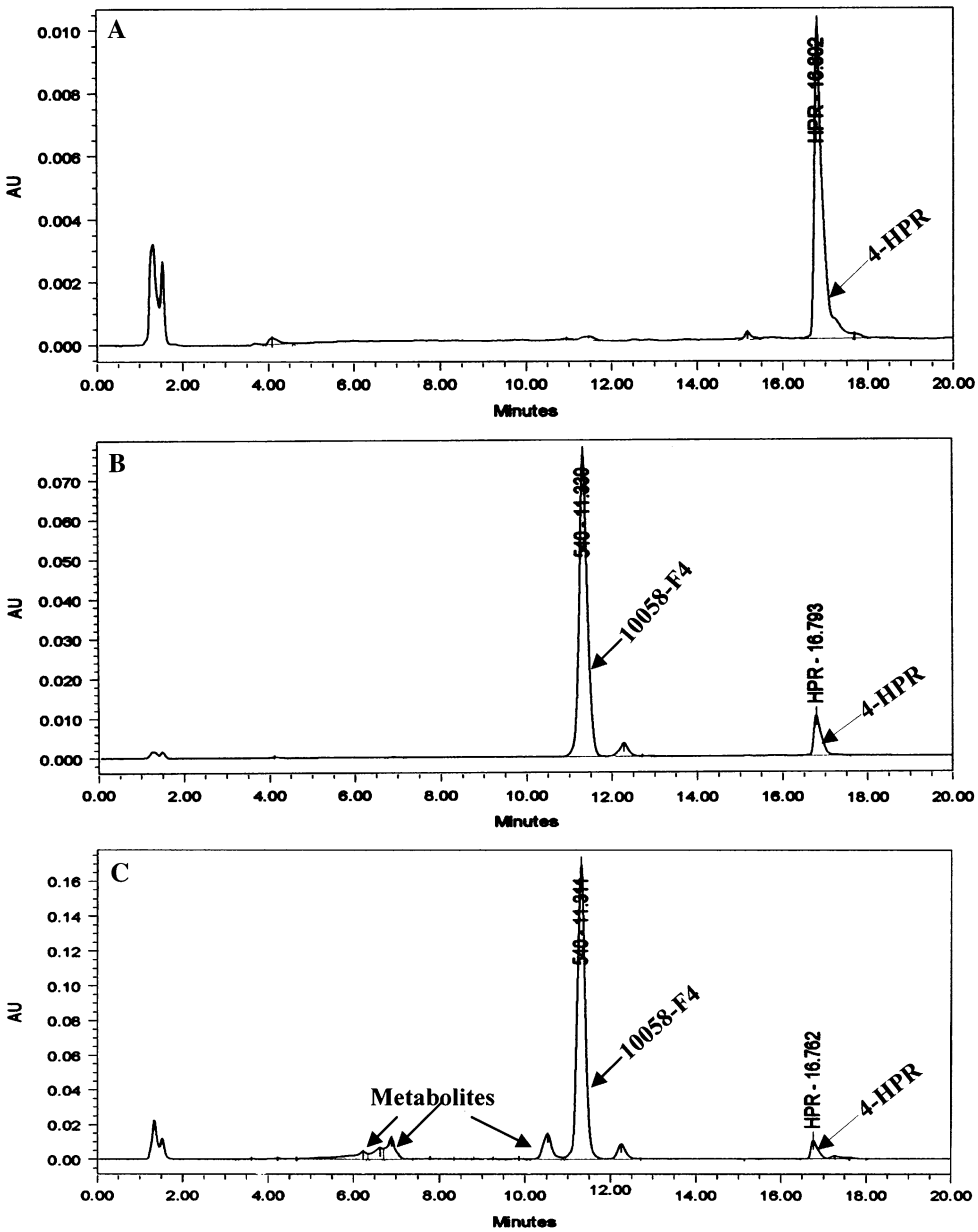

Fig. 3 HPLC chromatograms of 10058-F4 and metabolites in plasma. **a** Plasma obtained from a control animal with internal standard (fenretinide, 4-HPR) added, **b** the chromatogram of 10058-F4 added to plasma as a quality control assay standard, **c** the chromatogram of 10058-F4 and metabolites in plasma obtained 30 min after treating a mouse with 20 mg/kg of 10058-F4 i.v.

include RNA, siRNAs, dsRNAs, and poly-DNP-RNA [19–23]. In an animal study, the loss of the c-Myc phenotype blocked tumorigenesis, and transient inactivation of c-Myc increased the survival of mice bearing c-Myc dependent tumors [19]. However, in the study by Wang et al. the MCF-7 cells were transfected with the plasmids containing the shRNAs prior to implantation into the nude mice, and the cells with inactivated c-Myc did not grow [21].

In several in vitro studies, 10058-F4 has shown promise as an inhibitor of c-Myc/Max interactions. In three Burkitt's lymphoma cell lines and in one B-lymphoblastoid cell line, the GI_{50} value for 10058-F4 ranged from 23 to 60 μM [7]. Huang et al. reported that 10058-F4 could inhibit the growth of HL-60 acute myloid leukemic cells, with an IC_{50} of approximately 60 μM [8]. Similar inhibition was observed in HepG2 cells after exposure to 100 μM 10058-F4 for 24 h [8]. While our study was in progress, Wang et al. [24] examined structural analogs of 10058-F4 and found that one analog was about twofold more potent than 10058-F4 in inhibiting the growth of HL-60 cells in vitro; the IC_{50} of 27HR was 23 μM compared to 51 μM for 10058-F4. As an initial attempt to evaluate the therapeutic potential of 10058-F4, we evaluated the pharmacological properties, including the efficacy of 10058-F4 in mice. Androgen-independent prostate cancer cell lines were chosen as the xenograft model, because there is an enormous unmet need to develop additional therapeutics for this disease, in which c-Myc expression is elevated. Both DU145 and PC-3 cell lines are androgen-independent prostate cancer cell lines that constituatively overexpress c-Myc

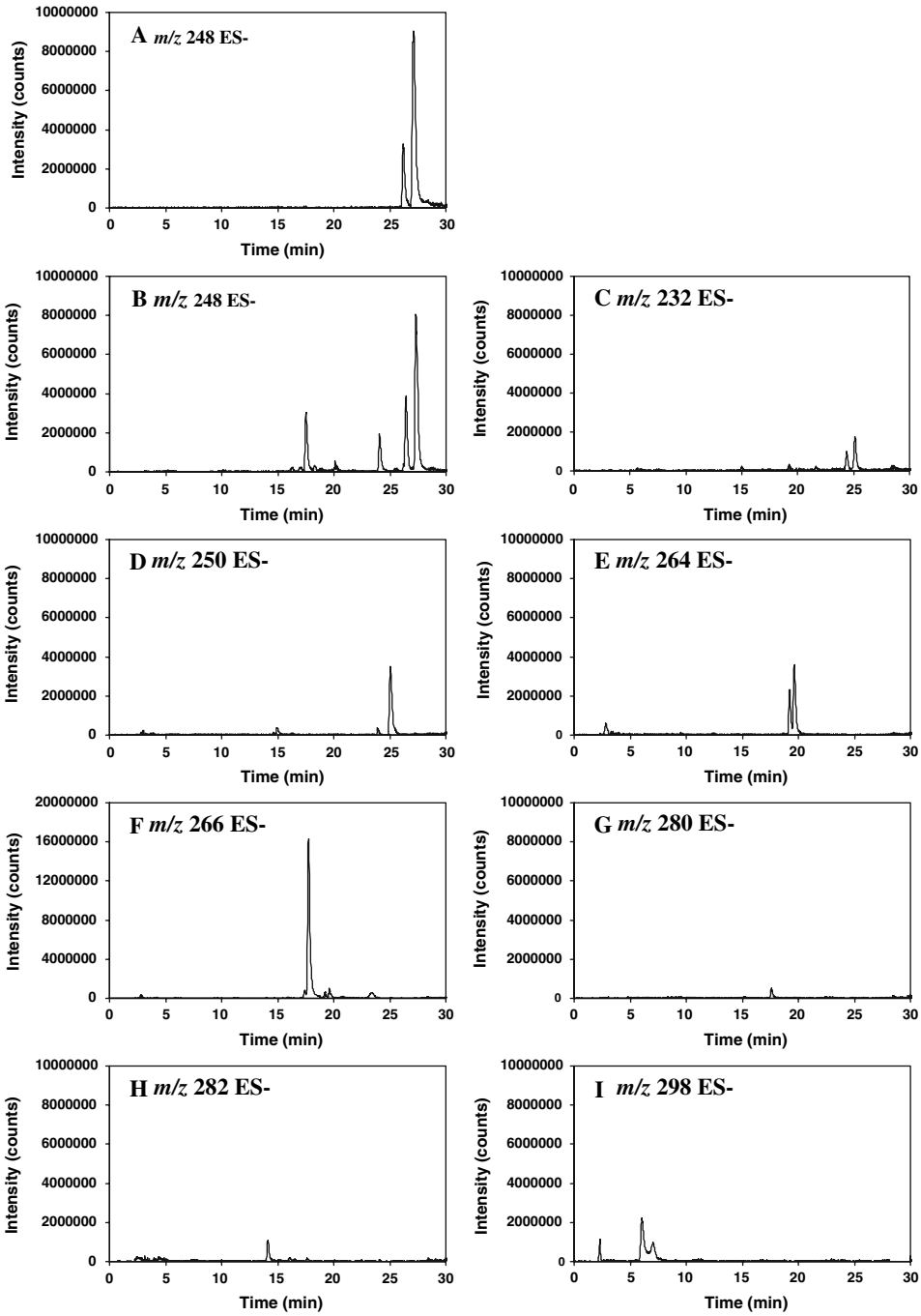

Fig. 4 Chromatograms of multiple reaction monitoring traces of potential metabolites of 10058-F4. **a** The chromatogram of parent compound 10058-F4 and contaminant. The retention time of 10058-F4 is 27 min and retention time of the contaminant is 26 min, **b–i** chromatograms of metabolites from either plasma or liver obtained 30 min after the mouse was treated i.v. with 20 mg/kg of 10058-F4. In B, parent compound, contaminant and additional metabolites with *m/z* of 248 are present. **c** Metabolites with *m/z* of 232; **d** metabolites with *m/z* of 250; **e** metabolites with *m/z* of 264; **f** metabolites with *m/z* of 266; **g** metabolite with *m/z* of 280; **h** metabolite with *m/z* of 282; **i** metabolites with *m/z* of 298

[25–27]. The m-RNA expression of PC-3 cells is 40% higher than that observed in the androgen-dependent prostate cancer cell line LNCaP [28]. From our in vitro studies, the IC50 values of 10058-F4 in DU145 and PC-3 androgen-independent prostate cancer cells were 88 and 113 μM, respectively, which are in the range previously reported for 10058-F4 in different cell lines.

Even at the maximum tolerated daily dose of 30 mg/kg for 5 days each week for 2 weeks, there was no significant tumor growth inhibition. In the PC-3 xenografts, the maximum %T/C was only 72% compared with 20% for docetaxel administered every 7 days. Against the slower growing DU145 xenografts, the %T/C for 10058-F4, when compared to the vehicle control was similar, 85%. Again this marginal activity was not statistically significant and much less than the anti-tumor activity of docetaxel, which had a maximum %T/C of 2% after two doses administered 7 days apart.

We conducted pharmacokinetic, tissue distribution, and pharmacodynamic studies in C B-17 SCID mice bearing either PC-3 or DU145 xenografts to help clarify the reasons for the lack of efficacy. When 10058-F4 was administered

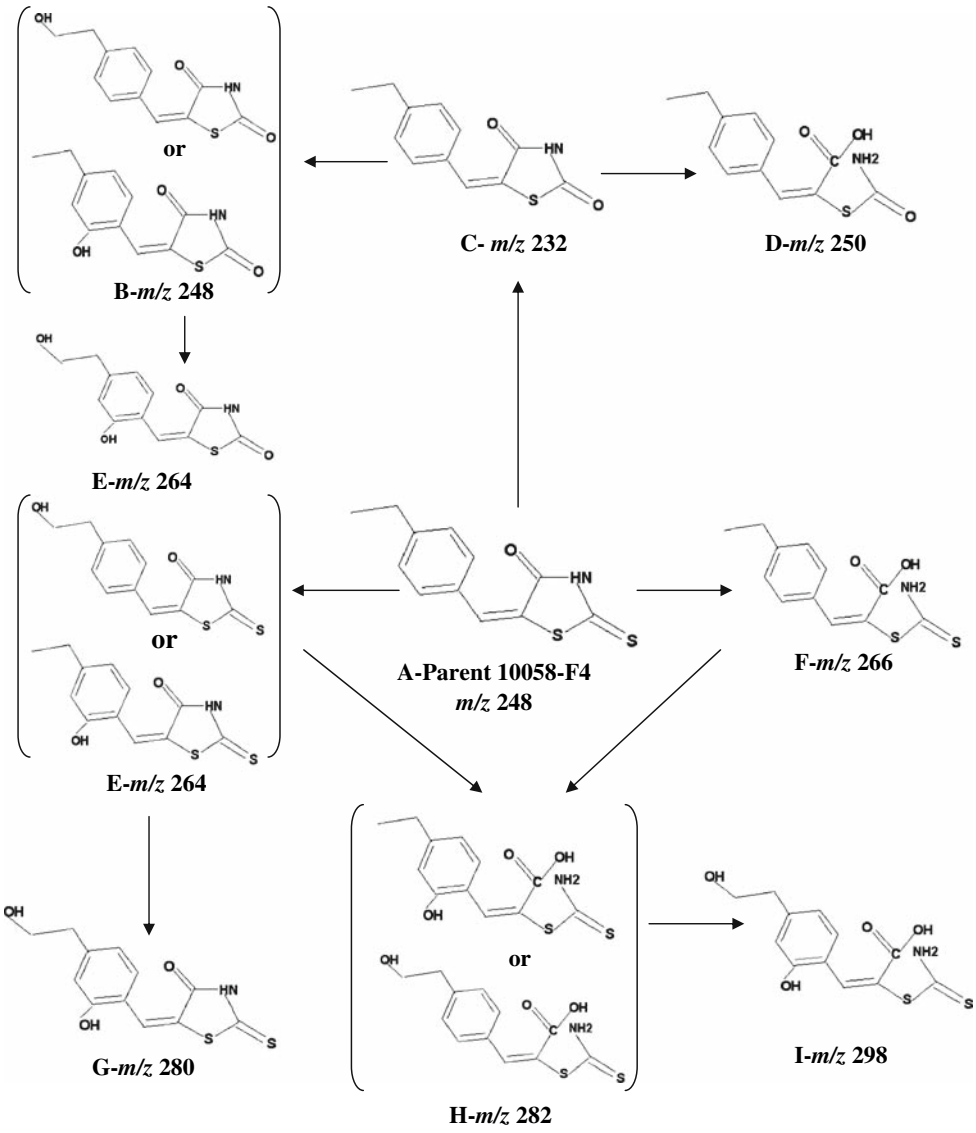

Fig. 5 Proposed metabolic fate of 10058-F4. Potential metabolites are listed alphabetically to correspond to the chromatograms presented in Fig. 4. The proposed structures are shown as well as the *m/z* ratios. The structure of 10058-F4 is shown as A-Parent in the center of the figure

as a single i.v. bolus at 20 mg/kg, the peak plasma concentrations at 5 min were about two- to threefold higher than the concentrations required for 50% inhibition of tumor cell growth in vitro. Nonetheless, the plasma half-life of 10058-F4 was only about 1 h, and by 6 h after dosing little, if any, 10058-F4 was detectable in plasma of mice bearing either PC-3 or DU145 xenografts. The rapid clearance of 10058-F4 was probably due to metabolism, in that little unchanged parent compound was detected in urine during the 24 h following dosing. When the tissue distribution of 10058-F4 was examined (Tables 2, 3), it was apparent that the concentrations of 10058-F4 present in tumor were only approximately 10 μM, which is much lower than the IC_{50} concentrations determined for these same cell lines in vitro. Further, 10058-F4 concentrations in all tissues except fat were less than those in plasma. Like the concentrations in plasma, tissue concentrations decreased rapidly and were not detectable at times beyond 6 h. Tumor exposure to 10058-F4, based on AUC, was only 10% of the plasma exposure in mice treated with 10058-F4 i.v.

The proposed metabolite structures based on *m/z* suggest that 10058-F4 was extensively metabolized.

Both c-Myc and Max were detected in all tumor samples, however, no changes in expression were observed in the tumors treated with 10058-F4. This lack of effect on total c-Myc protein in tumor tissues following treatment with 10058-F4 is most likely due to the five- to sixfold lower concentrations of 10058-F4 in tumor than the effective in vitro concentration [10]. The extensive metabolism and rapid clearance of 10058-F4 limit its usefulness as an effective small molecule inhibitor of c-Myc/Max in solid tumors after administration to animals. If effective concentrations of the inhibitor cannot be achieved at the target, the compound will be ineffective. Thus, as the quest for new small molecule inhibitors of c-Myc/Max continues, attention should be paid not only to in vitro potency, but also to

less metabolically labile compounds. Newer analogs [24] hopefully will have improved pharmacokinetic features.

Acknowledgments This study was supported in part by NIH CA78039 and DOD W81XWH-04-1-0226. We would like to thank Diane Mazzei and the staff of the DLAR for the excellent care of the animals and the UPCI writing group for their helpful suggestions regarding this manuscript.

References

1. Yin X, Giap C, Lazo JS, Prochownik EV (2003) Low molecular weight inhibitors of Myc/Max interaction and function. Oncogene 22:6151–6159
2. Blum KA, Lozanski G, Byrd JC (2004) Adult Burkitt leukemia and lymphoma. Blood 104:3009–3020
3. Shaffer AL, Wright G, Yang L, Powell J, Ngo V, Lamy L, Lam LT, Davis RE, Staudt LM (2006) A library of gene expression signatures to illuminate normal and pathological lymphoid biology. Immunol Rev 210:67–85
4. Berns EM, Klijn JG, Smid M, van Staveren IL, Look MP, van Putten WL, Foekens JA (1996) TP53 and MYC gene alterations independently predict poor prognosis in breast cancer patients. Genes Chromosomes Cancer 16:170–179
5. Schlotter CM, Vogt U, Bosse U, Mersch B, Wassmann K (2003) c-Myc, not HER-2/neu, can predict recurrence and mortality of patients with node-negative breast cancer. Breast Cancer Res 5:R30–R36
6. Arango D, Mariadason JM, Wilson AJ, Yang W, Corner GA, Aranes MJ, Augenlicht LH (2003) C-Myc overexpression sensitizes colon cancer cells to camptothecin-induced apoptosis. Br J Cancer 89:1757–1765
7. Gomez-Curet I, Perkins RS, Bennett R, Feidler KL, Dunn SP, Kruger LJ (2006) c-Myc inhibition negatively impacts lymphoma growth. J Pediatr Surg 41:207–211
8. Huang MJ, Cheng YC, Liu CR, Lin S, Liu E (2006) A small-molecule c-Myc inhibitor, 10058-F4, induces cell-cycle arrest, apoptosis, and myeloid differentiation of human acute myeloid leukemia. Exp Hematol 34:1480–1489
9. Lin CP, Liu JD, Chow JM, Liu CR, Liu HE (2007) Small-molecule c-Myc inhibitor, 10058-F4, inhibits proliferation, downregulates human telomerase reverse transcriptase and enhances chemosensitivity in human hepatocellular carcinoma cells. Anticancer Drugs 18:161–170
10. Sampson VB, Rong NH, Han J, Yang Q, Aris V, Soteropoulos P, Petrelli NJ, Dunn SP, Krueger LJ (2007) MicroRNA let-7a downregulates MYC and reverts MYC-induced growth in Burkitts lymphoma cells. Cancer Res 67:9762–9770
11. Gil J, Kerai P, Lleonart M, Bernard D, Cigudosa JC, Peters G, Carnero A, Beach D (2005) Immortalization of primary human prostate epithelial cells by c-Myc. Clin Cancer Res 65:2179–2185
12. Leonetti C, Biroccio A, D'Angelo C, Semple SC, Scarsella M, Zupi G (2007) Therapeutic Integration of c-Myc and bcl-2 antisense molecules with docetaxel in a preclinical model of hormone-refractory prostate cancer. Prostate 67:1475–1485
13. Nupponen NN, Kakkola L, Koivisto P, Visakorpi T (1998) Genetic alterations in hormone-refractory recurrent prostate carcinomas. Am J Pathol 153:141–148
14. McGiffie EM, Catapano CV (2002) Design of a novel triple helix forming oligodeoxyribonucleotide directed to the major promoter of the c-myc gene. Nucleic Acids Res 30:2701–2709
15. Berg T, Cohen SB, Desharnais J, Sonderegger C, Maslyar DJ, Goldberg J, Boger DL, Vogt PK (2002) Small-molecule antagonists of Myc/Max dimerization inhibit Myc-induced transformation of chicken embryo fibroblasts. Proc Natl Acad Sci USA 99:3830–3835
16. D'Argenio DZ, Schumitzky A (eds) (1997) ADAPT II user's guide: pharmacokinetic/pharmacodynamic systems analysis software. University of Southern California, Los Angeles
17. Akaike H (1979) A Bayesian extension of the minimal AIC procedures of autoregressive model fitting. Biometrika 66:237–242
18. Rocci ML, Jusko WJ (1983) LAGRAN program for area and moments in pharmacokinetic analysis. Comput Programs Biomed 16:203–216
19. Jain M, Arvanitis C, Chu K, Dewey W, Leonahardt E, Trinh M, Sundberg CD, Bishop M, Felsher DW (2002) Sustained loss of a neoplastic phenotype by brief inactivation of MYC. Science 297:102–104
20. Cutrona G, Carpaneto EM, Ponzanelli A, Uliva M, Millo E, Scarfi S, Roncella S, Benatti U, Boffa LC, Ferrarini M (2003) Inhibition of the translocated c-myc in Burkitt's lymphoma by a PNA Complementary to the Eμ Enhancer. Cancer Res 63:6144–6148
21. Wang YH, Liu S, Zhang G, Zhou CQ, Zhu HX, Zhou XB, Quan LP, Bai JF, Xu NZ (2005) Knockdown of c-Myc expression by RNAi inhibits MCF-7 breast tumor cells growth in vitro and in vivo. Breast Cancer Res 7:R220–R228
22. Shen L, Zhang C, Ambrus JL, Wang JH (2005) Silencing of human c-myc oncogene expression by poly-DNP-RNA. Oligonucleotides 15:23–35
23. Siddiqui-Jain A, Grand CL, Bearss DJ, Hurley LH (2002) Direct evidence for a G-quadruplex in a promoter region and its targeting with a small molecule to repress c-Myc transcription. Proc Natl Acad Sci USA 99:11593–11598
24. Wang H, Hammoudeh DI, Follis AV, Reese BE, Lazo JS, Metallo SJ, Prochownik EV (2007) Improved low molecular weight Myc–Max inhibitors. Mol Cancer Ther 6:2399–2408
25. Xiao D, Qu X, Weber C (2002) GRP receptor-mediated immediate early gene expression and transcription factor Elk-1 activation in prostate cancer cells. Regulatory Peptides 109:141–148
26. Cassinelli G, Supino R, Zuco V, Lanzi C, Scovassi AI, Semple SC, Zunino F (2004) Role of c-myc protein in hormone refractory prostate carcinoma: cellular response to paclitaxel. Biochem Pharmacol 68:923–932
27. Bernard D, Pourtier-Manzanedo A, Gil J, Beach DH (2003) Myc confers androgen-independent prostate cancer cell growth. J Clin Invest 112:1724–1737
28. Yoshimura I, Wu JM, Chen Y, Ng C, Mallouh C, Backer JM, Mendola CE, Tazaki H (1995) Effects of 5-α-Dihydrotestosterone (DHT) on the transcription of nm23 and c-myc genes in human prostatic LNCaP cells. Biochem Biophy Res Commun 208:603–609